IOP Publishing Measurement Science and Technology
Meas. Sci. Technol. **31** (2020) 065301 (13pp) https://doi.org/10.1088/1361-6501/ab75b1

Oil droplet sizing and velocity determination using a fiber-optic reflectometer

Jitae Do[1], Wei-Liang Chuang[2] and Kuang-An Chang[1,3]

[1] Department of Ocean Engineering, Texas A&M University, College Station, TX 77843, United States of America
[2] Department of Marine Environment and Engineering, National Sun Yat-sen University, Kaohsiung 804, Taiwan
[3] Zachry Department of Civil and Environmental Engineering, Texas A&M University, College Station, TX 77843, United States of America

E-mail: kchang@tamu.edu

Received 1 October 2019, revised 24 January 2020
Accepted for publication 12 February 2020
Published 13 April 2020

Abstract

This study attempts to apply a single-probe fiber-optic reflectometer (FOR) to determine the velocities and sizes of oil droplets rising in a static water column. The concept proposed by Chang *et al* (2003 *Rev. Sci. Instrum.* **74** 3559–65) was employed to derive the oil droplet velocity from a signal acquired using the FOR technique. An oil plume in a vertical water column was set up to verify the applicability in the oil–water mixture flow. A high-speed imaging technique was applied to provide control data sets for quantitative validation. The droplet velocity, residence time, and chord length measurements were validated by comparing with the results from high-speed images using the bubble image velocimetry technique and the image gradient method. To extract the oil-phase residence time, a double-threshold method was applied. It was found that the velocity measured by the FOR probe has an error of approximately 8%, while the measured chord length has an error of 13% and 8% in direct and indirect comparison with images, respectively. Furthermore, to evaluate the applicability of droplet size estimation using the present cleaved-tip single-optical-fiber probe, droplet–probe interaction was studied to examine the lower limit of the measurable range using dominant dimensionless parameters. The lower limit was found as roughly 20 times the diameter of the optical-fiber probe.

Keywords: oil droplet, droplet velocity, droplet sizing, chord length, fiber-optic probe

(Some figures may appear in colour only in the online journal)

1. Introduction

Oil droplet sizing is a common challenge in various disciplines, such as petroleum engineering, chemical engineering, food science, and the pharmaceutical industry. The technique for measuring oil droplet size distribution is consistently being developed or improved by engineers and scientists. Not limited to land, oil droplet sizing is also of great interest in ocean environmental studies, particularly the oil and gas blowout on the sea floor at deep water level. When oil is released in deep water and breaks up into droplets, owing to buoyancy and surface tension, larger droplets with diameters of $O(1\ \text{mm})$ may rise and reach the sea surface faster, resulting in oil slick formation, while the smaller ones with diameters of $O(1\ \mu\text{m})$ tend to rise more slowly and can be transported long distances from the discharge location [1]. As a result, the oil droplet size distribution is a very important factor in the fate of oil in an ocean environment. Understanding of both the physical and chemical properties of the distribution are generally expected to provide necessary knowledge to the development of countermeasures.

To measure oil droplet size, optical techniques are often viewed as the most robust approaches with the advantage of non-intrusiveness. The optical techniques can be typically

categorized into two methods: imaging methods and light-scattering methods. The imaging method is to extract the droplet size from captured images by applying image processing or analysis schemes. For example, Tan and Yao [2] conducted an experiment in the laboratory to measure the distribution of oil droplets in a water column from laser-illuminated images. In that particular experiment, they found that 98% of oil droplets were less than 78 μm and the maximum diameter of the dispersed oil droplets was 113 μm. The imaging method was also employed with a combination of remotely operated vehicle (ROV) and video cameras to obtain the *in-situ* oil droplet size distribution from a field experiment in which gas and oil mixtures were released from a depth of 844 m at 125 km off the coast of central Norway [1]. In the report, the maximum droplet diameter was 8–10 mm and the oil droplets with diameter greater than the critical diameter no longer increased with droplet size.

A light-scattering method may be preferred when a higher data rate and more detailed statistical properties are desired. For the scattering methods, a laser is typically employed in combination with an optical transmitter and an optical receiver which collects light scattered by droplets passing through the sampling volume. Lunel [3] conducted a field experiment to measure the oil droplet size distributions below oil slicks using a phase Doppler particle analyzer (PDPA) with a measurable range of 1–300 μm. Lunel found that the mean droplet diameter was no greater than 50 μm and the maximum droplet size was around 100 μm. More recently, laser *in-situ* scattering and transmissometry (LISST) was employed for oil droplet size measurement in the laboratory to study droplet breakup and effectiveness of dispersant injection on a small scale [4] and a large scale [5] with a measurable range from 2.5 to 500 μm in diameter. With an upper detection limit of 500 μm, a significant droplet size fraction was reported outside the measurable range in some cases [4]. Another application of the scattered methods is in the focus beam reflectance method (FBRM). The measurement principle of FBRM is based on backward light scattering using a focused beam of laser light that scans across a particle passing in front of the probe window to take measurements. Boxall *et al* [6] conducted measurements of droplet size distribution in water-in-oil emulsions using FBRM compared with a particle video microscope. They concluded that water droplets with diameter up to 2 mm can be measured with a typical average error of less than 20% when using FBRM.

Although several successful applications of both imaging methods and light-scattering methods for measuring oil droplet size distribution have been reported, both methods are subject to overlapping interference when the droplets are in high concentration. Furthermore, the scattering methods have an upper limit which is not adequate to cover a wide range of droplet sizes in the order of 1 mm in diameter. More importantly, these methods do not provide the droplet velocity distribution. For such purposes, intrusive probes may be preferred.

For intrusive probes, conductivity probes [7–10] and optical-fiber probes [11–26] have been utilized for several decades to estimate the size, velocity, and volumetric fraction of air bubbles. The conductivity probes utilize the difference in electrical conductivity, while the optical-fiber probes detect the transition between different refractive indices. Comparing between conductivity and optical-fiber probes, the optical-fiber probes are generally preferred since their signal-to-noise ratio and sensitivity are much higher than those of the conductivity probes [24]. Furthermore, the optical-fiber probes have the advantages of simplicity of use, near non-intrusiveness due to their miniature dimensions (of the order of 100 μm), and very short response time (of the order of 10 ns).

Intrusive probes have been successfully employed in the study of aerated flows. In these applications, obtaining the air-phase residence time (and therefore the air volumetric fraction) is relatively straightforward but determining the bubble velocity is not. To determine the air bubble velocity, dual [19, 27–29] or quadruple [24–26] optical-fiber probes are commonly applied and the probe signals are cross-correlated. However, the use of multiple probes may alter or even break up the air bubble formation. In such cases, the probe configuration becomes a challenge in which its interference to the flow must be minimized. Furthermore, the interaction between rising air bubbles and multiple optical-fiber probes may disturb velocity measurements [27, 28]. The influence may result in large uncertainty in the velocity estimation and in turn affect the measured chord length and volumetric fraction. To overcome these issues [20], proposed the fiber-optic reflectometer (FOR) technique, which only requires a single optical-fiber probe to derive air bubble as well as seeding particle velocities. Lim *et al* [23] further extended the technique to measure sizes of air bubbles in an aerated flow.

Compared to the literature on air bubble sizing and velocity determination using conductivity or optical-fiber probes, the number of studies on oil droplet sizing and velocity determination in oil–water mixture flows is relatively limited. Among some valuable works [30–33] employed dual conductivity probes to measure the velocity, volumetric fraction, and size distribution of oil droplets. Using a single cleaved optical-fiber probe [34], first demonstrated the possibility of measuring oil-phase residence time in a vertical kerosene–water mixture flow. Subsequently [35], applied dual optical-fiber probes to measure velocity and estimate oil droplet size. Hamad and He [36] later reported a validation study by comparing the results obtained by hot-film probe, further confirming the feasibility of measuring velocity, volume fraction, and droplet size with dual optical-fiber probes. More recently [37, 38] employed quadruple optical-fiber probes to measure the size and three-dimensional velocity of oil droplets. In the process, a rather complicated algorithm based on two assumptions is required to complete the measurements. They assumed that (i) the velocity and size of droplets are constant during the probe penetration, and (ii) the oil droplets are spherical. Such assumptions allow the measurable droplet size to be up to 4 mm in diameter.

To the authors' knowledge, the examination of oil droplet sizing and velocity determination using a single optical-fiber probe with its range of applicability and intrusive effects remains unattempted. As mentioned earlier, obstruction by the intrusion of the probes, although small in dimensions, remains a concern due to the viscous nature of the oil droplets. The less intrusive nature of the single-probe approach thus features

great advantages over the multiple-probes setting. Hence, the success of using a single fiber-optical probe for simultaneous velocity and size measurements of oil droplets in an oil–water mixture flow would be promising.

This study aims to develop an optical-fiber-based technique with a single probe for measuring the velocity, residence time, and size of oil droplets in oil–water mixture flows. It employed the FOR technique developed by Chang *et al* [20] and extended the velocity and size measurements of air bubbles proposed by Lim *et al* [23] in a bubble plume to those of oil droplets in an oil plume rising in an otherwise static water column. An oil plume in a vertical water column was set up to examine the technique. A high-speed imaging technique was employed to provide control data sets for quantitative validation. This paper is organized as follows: (i) experiment condition and principle of FOR; (ii) derivation and validation of oil droplet velocity; (iii) validation of residence time and chord length measurements; (iv) discussion on droplet–probe interaction to investigate the limit of measurable range using this technique. These are then followed by conclusions to summarize the findings of the study.

2. Experiment condition and principle

2.1. Experiment condition

A square-cross-section water column with oil released by four nozzles at the bottom was set up to test the FOR technique. The test condition simulates an underwater oil plume in a confined space. Figure 1 illustrates the experimental setup, including the optical-fiber probe, high-speed photography, and the constant-head configuration for maintaining a constant pressure head (in both the water column and the reservoir) and oil flow rate. The oil employed in this study is Penreco Conosol C-200, and its physical properties, as provided by the manufacturer, that are essential to the FOR application are listed in table 1. The acrylic square column, with a wall thickness of 4 mm, has dimensions of 1000 mm height and 50 mm width. Before releasing oil in each test, the column was filled with water to a depth of 693 mm. The oil flow rate was regulated by an electronically controlled pump that connects an oil reservoir and a one-to-four splitting tube evenly distributing the oil flow to the four nozzles. The nozzles, with circular openings, were evenly located at the four corners of the column. The center of each nozzle is 10 mm from each side of the inner column wall. An opening on one of the column walls 100 mm below the top was designed to allow overflow of oil to return to the reservoir. Through this, the fluid head and the oil flow rate were kept constant throughout the experiment.

Oil droplets were generated by the nozzles with four different inner diameters: 3, 2, 1, and 0.5 mm (hereafter termed as Cases I, II, III, and IV, respectively). The setup of the optical-fiber probe followed the method in Chang *et al* [20], in which the velocity and residence time of rising air bubbles in a bubble plume were measured using a single optical-fiber probe. The optical-fiber probe was fixed pointing vertically downwards with its tip at 634 mm above the column bottom. As the oil plume was confined by the narrow column, the droplets had

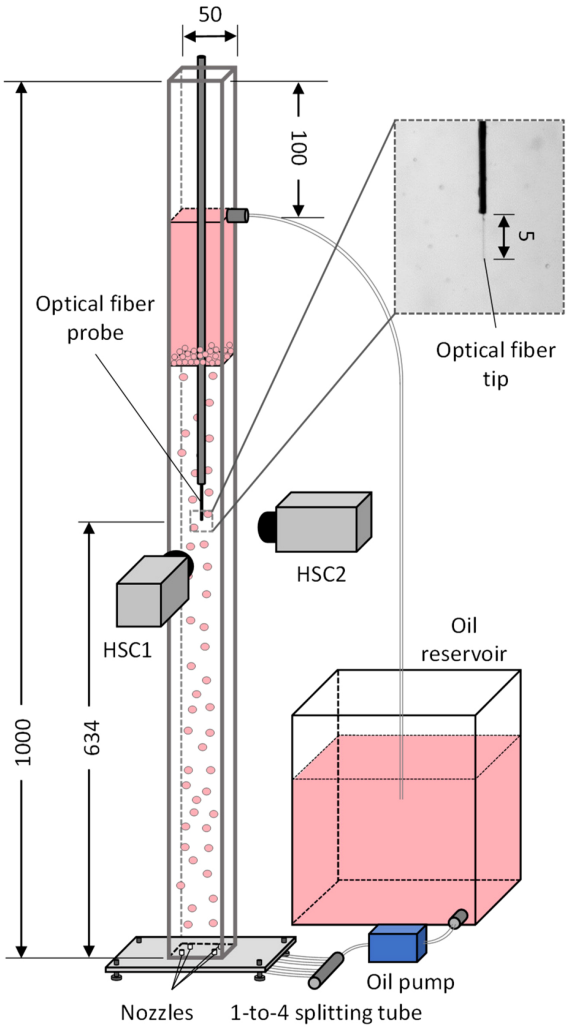

Figure 1. Schematic diagram of the experimental setup for measuring the rising oil droplets using FOR and imaging. Note that HSC indicates a high-speed camera, and the diagram is not to scale. The units are in mm.

been homogenously distributed before reaching the measurement position, confirmed by visual examination and inspecting camera images. A needle made of stainless steel with an inner diameter of 1 mm was used to direct and support the optical fiber. The fiber end tip protruded out of the needle by 5 mm to avoid oil residue around the needle end, while the optical fiber remained sufficiently stiff when encountering droplets. The setup followed previous FOR applications in violent wave impacts [39, 40], and was further verified by video examination in preliminary tests.

For visual examination and validation purposes, a high-speed imaging technique using two high-speed cameras (Vision Research Phantom M340) was employed and synchronized with the acquisition of the FOR signal. The side-looking arrangement for both cameras is also illustrated in figure 1. The center of each camera field of view (FOV) targets the fiber end tip, and the measurement planes are normal to each other. In doing so, the three-dimensional motion of oil droplets and the location of penetration when encountering the fiber tip can be

Table 1. Oil type and physical properties essential to FOR application.

Oil type	Density (kg m^{-3})	Kinematic viscosity (m^2 s^{-1})	Refractive index
Penreco Conosol C-200	818	2.36×10^{-6}	1.452

inferred. In the experiment, the camera framing rate was set to 500 frames per second. Both cameras were mounted with a Nikon Micro-Nikkor 60-mm f/2.8D lens with an f stop of f/8.0. The FOVs were set to 32×32 mm^2 for Case I and 34×34 mm^2 for Cases II, III, and IV. The camera has a resolution of 1024×1024 pixels. This results in a spatial resolution of 0.032 mm pixel^{-1} for Case I and 0.033 mm pixel^{-1} for Cases II, III, and IV, and depth of field (DOF) of 2.8 mm and 3.1 mm, respectively. Note that the FOVs cover approximately 80% of the inner flume width.

To measure velocity using a single optical-fiber probe, a very high sampling rate is required. This was achieved by using a high-speed digitizer (NI 5112, National Instruments), while 5 MHz was estimated to be a sufficient sampling rate (details to follow). Due to the memory limitation in the high speed cameras, only 15 s of time series data were recorded when using such a high sampling rate. To acquire a sufficient number of oil droplet encounters for subsequent analysis, 40 repeated tests were conducted consecutively for each of the four cases, leading to a 600 s equivalent recording length based on the well-mixing condition for each case. Table 2 summarizes the test conditions with the nozzle size, number of droplet encounters, droplet encounter frequencies, fraction ratio from phase transition measured by FOR signals, and average diameters of droplets obtained from the high-speed images. Note that an edge-detection technique using Canny edge detector was performed to measure the area and thus the average diameter of the droplets.

2.2. Principle of FOR technique

In this study, the FOR technique proposed by Chang *et al* [20] was applied. The light source of the technique was a multilongitudinal-mode diode laser with a 1 mW output power and 1310 nm wavelength (λ). The optical waves sent from the laser are then divided by a 2×2 single-mode fuse fiber coupler with a splitting ratio of 50:50. Two paths from the coupler lead the optical waves to two optical fiber patches—one terminated as a flat-cut end tip and the other terminated as an angled physical contact (APC). The APC end serves as a reference, while the flat-cut end tip serves as the probe end. Note that the flat-cut end tip was processed by a cleaver that ensures a normal angle surface at the fiber end tip. The SMF-28 (single-mode fiber-28), a standard telecommunications-grade optical fiber, was used in this study. The SMF-28 fiber has a core dimeter of 8 μm cladded by a protection layer with a diameter of 125 μm. The detected signal is acquired by a high-speed digitizer.

The amplitude of the detected signal represents the reflected optical power due to Fresnel reflections off the fiber–fluid interface at the fiber tip. The power of light reflected from the fiber–fluid interface using Fresnel reflectivity can be expressed as

$$P_1 = P_0 \alpha^2 \mathcal{R}; \mathcal{R} = \left(\frac{n - n_f}{n + n_f} \right)^2 \quad (1)$$

where P_1 is the detected power of the light reflected from the fiber–fluid interface, P_0 is the laser power (1 mW), α is the splitting ratio of the fiber coupler ($\alpha = 0.50$), $\mathcal{R}$ is the Fresnel reflectivity, and n_f is the refractive index of the optical fiber ($n_f = 1.444$). Note that the n value of pure water (n_w) and Penreco Conosol C-200 oil (n_o) are 1.333 and 1.452, respectively.

2.3. FOR signal signature in oil droplet encounter

Figure 2 shows a sample raw FOR signal with 13 encounters of oil droplets together with a pair of snapshots captured by the two high-speed cameras, HSC1 and HSC2, which visualize one of the oil droplet encounters. Unlike the always-positive square-like FOR signals in a bubble plume reported by Lim *et al* [23], positive, negative, and fluctuating as well as non-bell-shaped oscillating signals were all observed as demonstrated in figure 3. It should be noted that signals in 27% of the encounters were found to be of negative, square-like signal type, while a similar proportion of 25% of the encounters were of oscillating signal type. As a result, the typical crossing method with a single threshold used in bubble identification is insufficient to identify the oil droplet encounters. Before discussing the signals in detail, it is worth pointing out that [41] discussed the wetting film effect on a cleaved-tip optical-fiber probe. They reported that the measured reflectivity, when it is immersed in the non-wetting phase, fluctuates according to the thickness of water wetting film and possibly the inclination of the wetting film. Applying standard thin-film theory [42] to equation (1) can be expressed as follows:

$$P_2 = P_0 \alpha^2 \mathcal{R}'; \mathcal{R}' = \left(\frac{n n_f - n_w^2}{n n_f + n_w^2} \right)^2 \quad (2)$$

where n, n_f, and n_w are the refractive indices of the dispersed phase (oil for the present study), optical fiber, and water film wetting on the optical fiber tip, respectively, and $\mathcal{R}'$ is the corresponding Fresnel reflectivity.

Table 3 summarizes the reflected power P_1 and P_2 calculated using equations (1) and (2), and power changes ΔP_1 and ΔP_2 from the continuous phase (water). If the wetting effect of the thin film on the tip is large, the power change from oil to water, ΔP_2, is positive, as shown in figure 3(a). If the effect is small, the power change from oil to water, ΔP_1, is negative, as shown in figure 3(b). A fluctuating signal in the oil phase is also observed, as shown in figure 3(c). This could imply the wetting water film thickness may change during penetration. Sun *et al* [38] also observed the negative and fluctuating signals in 40% octanol–kerosene and water mixture flow. For non-bell-shaped oscillating signals as shown

Table 2. Test conditions.

Test	Nozzle inner diameter (mm)	No. of encounters	Encounter frequency (s^{-1})	Fraction ratio (%)	Average diameter (mm)
Case I	3	1562	2.6	6.1	6.6
Case II	2	1671	2.6	5.3	4.8
Case III	1	1150	1.9	3.0	3.3
Case IV	0.5	157	0.6	0.3	1.6

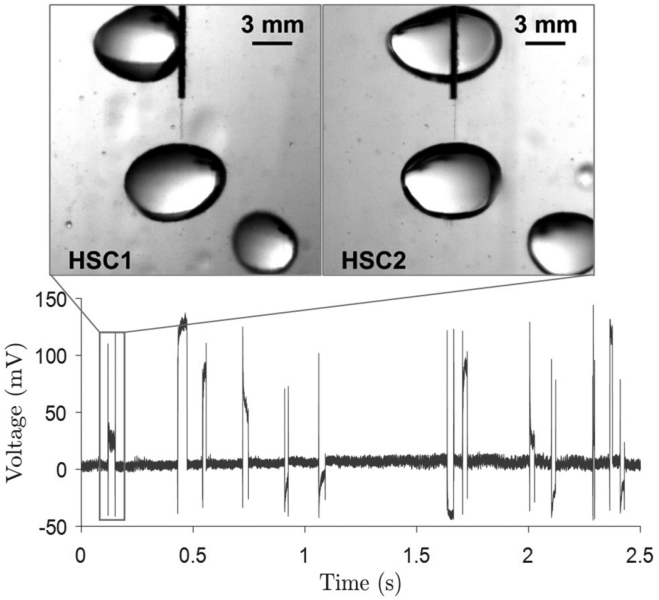

Figure 2. Sample raw FOR signal with 13 encounters of oil droplets, and images from HSC1 and HSC2 for a sample droplet encounter with the fiber end tip.

in figure 3(d), Lim *et al* [23] reported that the oscillating signal emerges when the penetration occurs around the lateral side of the air bubbles and the pattern of the oscillating signal is bell-shaped. Our visual examination confirmed that similar signal patterns applied to oil droplets but the shape of the signal was not bell-shaped. Compared to the FOR signal from air bubbles in the water column [23], the appearance of negative signals, fluctuating signals, and non-bell-shaped oscillating signals was notably different. This wetting film issue may not be a problem for air bubble signals since the power change from the air (water film) to water phase is much higher than the reflected power in the water phase, while the wetting issue would not be negligible in oil–water mixture flows since the power change from oil (water–film) crosses over the reflected power in the water phase. This also implies that the single-threshold detection method may fail to discriminate between the oil and water phases. This will be discussed in section 4 in detail.

3. Determination of oil droplet velocity

3.1. Principle

In an air-bubble plume [20], reported that, shortly before the fiber tip is in contact with an air bubble and the contact angle is nearly normal to the optical fiber end-tip surface, a coherent-beat signal was received by the FOR probe. This oscillatory signal is the result of coherent mixing of scattered signal from the bubble with Fresnel reflection signal from the tip of the optical fiber. The period of the signal provides necessary information to determine the air bubble velocity. The same concept may be applicable to measuring the oil droplet velocity. This section will demonstrate the works that follow the algorithm and application elucidated by Chang *et al* [20] and Lim *et al* [23], as well as the validation by comparing with the result measured by bubble image velocimetry [43].

According to Chang *et al* [20], the velocity determination of an approaching interface by the oscillation signature can be formulated as

$$u = \frac{\Delta d}{T} \tag{3}$$

where T is the period of the oscillation, and Δd is the travel distance of the interface for one complete oscillation cycle, or

$$\Delta d = \frac{\lambda}{2n_w} \tag{4}$$

where λ is the laser wavelength ($\lambda = 1310$ nm), and n_w is the refractive index of water ($n_w = 1.333$). In this study, Δd was calculated as 492 nm.

3.2. Determination of oil–water interface velocity

A very high sampling rate of $O(1$ MHz) is required to reveal the signature of periodic oscillation in the FOR signal acquisition. Based on Chang *et al* [21], the minimum required sampling rate, determined by the Nyquist frequency, is approximated as $4|u_e|$ MHz where u_e is the maximum expected velocity in m s^{-1}. Figure 4(a) presents a FOR signal with the coherently mixing feature, as shown in its close-up in figure 4(b), of an oil droplet encounter. Indeed figure 4(a) is the close-up of the signal at around $t = 120$ ms in figure 3(a). It should be pointed out that the presence of analyzable oscillation signature in the FOR signal highly relies on the location of penetration. For example, figure 3(a) shows an ideal penetration scenario—the fiber tip approached and then pierced roughly at the center of the curved interface of an oil drop as the droplet was rising in the water column. As shown in Lim *et al* [23], an encounter position too far from the center of an air bubble tends to result in weak reflective signals that in turn would create poor oscillation signature and hamper its velocity determination. Such a critical condition considerably limits the number of analyzable signals over detected

Table 3. Reflected power and power changes.

P_1 (μW)			P_2 (μW)		ΔP_1 (μW)		ΔP_2 (μW)	
Water	Oil	Air	Oil (water film)	Air (water film)	Oil–water	Air–water	Oil (water film)–water	Air (water film)–water
0.39	0.003	8.13	1.32	2.63	−0.39	7.74	0.92	2.23

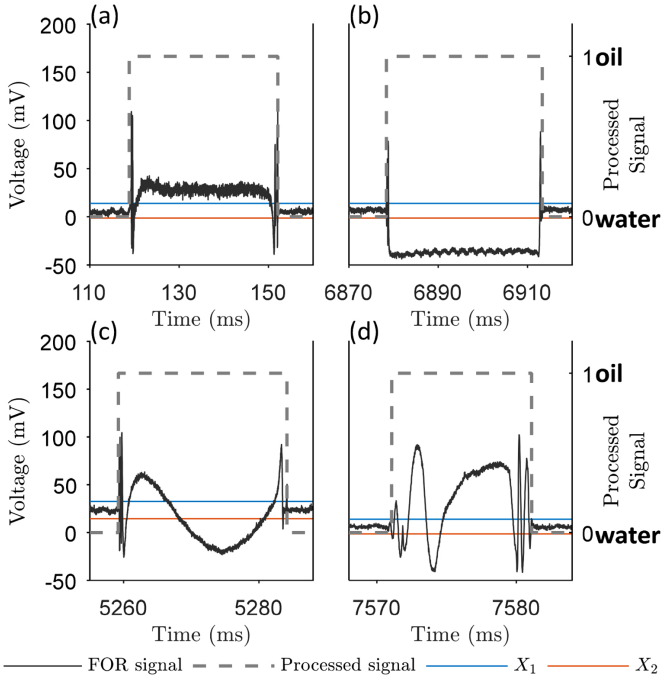

Figure 3. Three general types of FOR signal in oil droplet encounters: (a) positive square-like signal, (b) negative square-like signal, (c) fluctuating signal, (d) non-bell-shaped oscillating signal. The 'high pulses' in (a), (b) and (c) were the results of droplets approaching the fiber end tip and, after penetration, leaving the fiber tip. Note that X_1 and X_2 represent the upper and lower thresholds applied in the signal processing, respectively.

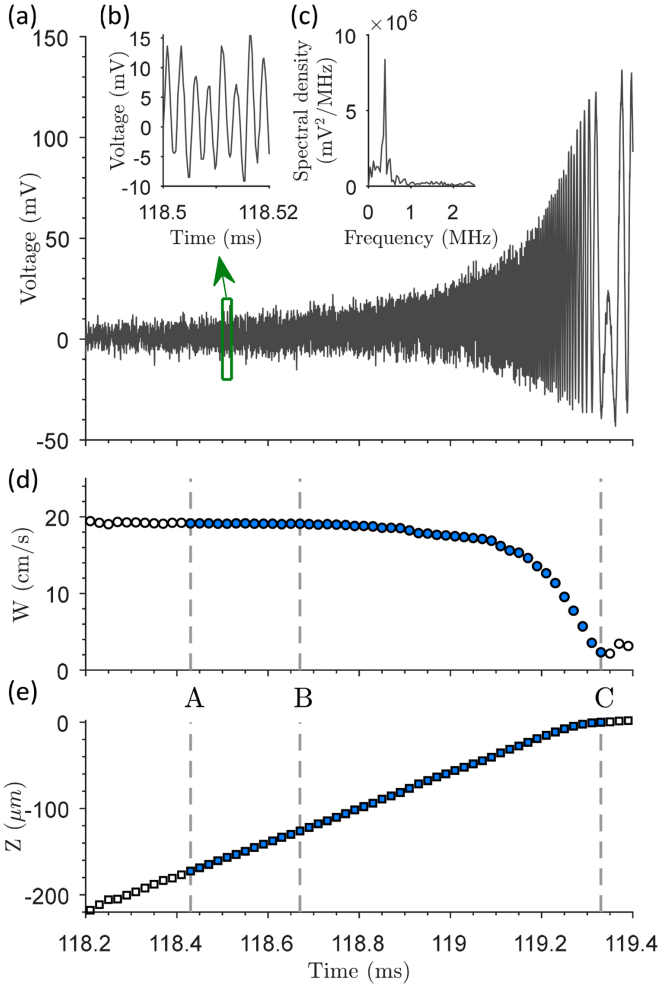

Figure 4. Description of oil droplet velocity determination. (a) Close-up of the rising signal in figure 3(a). (b) Close-up of a randomly selected 20 μs segment. (c) Spectrum of the signal in (b). (d) Resulting velocity corresponding to the signal in (a). (e) Corresponding displacement of the oil droplet with $z = 0$ being the end face of the fiber tip. Note that the time moments *A*, *B* and *C* correspond to $z = -175$, -125, and 0 μm, respectively.

droplet events. Nevertheless, the limitation also implies all effective encounters occurred when the probe is piecing nearly through the center of the droplets. Accordingly, the resulting chord length, which can be calculated through the measured velocity and residence time, does not deviate too far from the actual diameter of the droplet. This chord length may in turn be used to present the diameter of the droplet with uncertainty to be quantified in the next section.

For the oil droplets effective for velocity determination, the experiment counted 14 out of 1562 (or 0.9%), 18 out of 1671 (or 1.1%), and 11 out of 1150 (or 1.0%) for Cases I, II and III, respectively. Overall, the rate of analyzable encounters is approximately 1% for oil droplets, mainly due to the low probability of center-piecing events. Since there is no analyzable signal in Case IV, processing for velocity measurement was not performed in Case IV. The main cause is its small droplet size; more discussion will follow in section 5. Compared to the air bubble velocity determination by Lim *et al* [23], the proportion of analyzable encounters is roughly 50% lower than that for air bubbles (roughly 2%). Since the oil–water surface tension is about one-third of the air–water surface tension, oil droplets tend to deform more easily than air bubbles. The deformation of oil droplets could contribute to the reduction in the number of analyzable encounters. It is also worth noting that the coherent-beat signals were also observed when the optical fiber leaves the oil droplets and pierces through the near center, similar to that reported in Lim *et al* [23] for air bubbles. However, those signals were excluded for oil droplet velocity determination since the viscous effect could

create a higher uncertainty in comparison to its front-surface encounter.

The oscillation period T is needed to calculate the droplet velocity in equation (3). To find T, a constant interval of 20 μs (see figure 4(b)) was assigned to divide the oscillating signal into several time segments. The assignment of the constant interval was not randomly selected but determined by a convergence test. Figure 4(b) shows the received sample signal within a short duration of 20 μs, featuring several coherent beat waves. Fast Fourier transform (FFT) was then applied to the signal in each segment (see figure 4(c)) to find T by locating the peak frequency in the spectrum using a cubic-spline method. The same routine was applied to each time segment so the time series of the oil–water interface velocity, as presented in figure 4(d), can be obtained. As shown in figure 4(d), the droplet started to decelerate when it approached the fiber tip due to the viscous effect. The result is similar to that reported in Lim *et al* [23] for air bubble measurements.

3.3. Determination of oil droplet velocity

In principle, the most sensible distance for determining the velocity of an approaching object is subject to the laser emission power and interference (mainly due to the viscous effect of the flow) of the optical fiber. Chang *et al* [20] reported a more specific definition by considering the size of the optical fiber. They concluded that the (nearly constant) approaching velocity of air bubbles is sensed from 1.4 to 1 times the diameter of the fiber end face (i.e. $z = -(175-125)$ μm) as the object moves towards the fiber tip, and the average of the velocity data points within this range represents the object velocity. Lim *et al* [23] further gave a thorough description of how the interaction between the optical fiber tip and an approaching air bubble can affect the velocity determination. They also indicated that the velocity averaged over the range within $z = -(1.4–1)$ times the fiber diameter in front of the fiber end-tip face may represent the air bubble velocity. In the present study, the concept proposed by Chang *et al* [20] was used to determine the oil droplet velocity. To locate the arrival time at $z = -175$ and -125 μm (i.e. 1.4 and 1 times the fiber diameter) in front of the fiber end tip, namely points A and B in figure 4, the time series of the droplet displacement (figure 4(e)) should be determined. This can be simply done by integrating figure 4(d) over time. As a result, points A and B can be easily determined, and the oil droplet velocity can be readily obtained by averaging the data points within this interval.

3.4. Validation of oil droplet velocity measurement

To validate the oil droplet velocity derived from the FOR signal, the image-based bubble image velocimetry (BIV) technique introduced by Ryu *et al* [43] was employed. The technique is capable of quantifying multiphase flow velocity through cross-correlating successive images. Subsequently, the images captured by HSC1 and HSC2 were processed to obtain the velocity of the oil–water interface of a droplet. To resolve the motion of the deforming rim of the oil droplet, a final interrogation window of 16 × 16 pixels was selected, reducing from the initial interrogation window of 128 × 128 pixels in the multi-pass algorithm. With 50% overlap between adjacent interrogation windows, the velocity vectors have a fine spatial resolution of 0.26 mm × 0.26 mm.

The oil droplet velocity derived from the FOR signal has a temporal resolution of 20 μs, while the temporal resolution of BIV is only 2000 μs. To be able to compare the velocities measured by BIV and FOR, the BIV velocity (W_{BIV}) is extrapolated using two consecutive velocities before the optical fiber is in contact with the oil droplet to match up with the temporal resolution of the FOR velocity (W_{FOR}). Assuming the droplet velocity is linear in such a short duration, a linear extrapolation method was employed for BIV velocity calculation in the range from $z = -175$ to -125 μm before the optical fiber came into contact with the oil droplet. To evaluate the uncertainties in the comparison, the MBE (mean bias error), RMSE (root-mean-square error), MRE (mean relative error), and RMSRE (root-mean-square relative error) were calculated as follows:

$$\mathrm{MBE} = \frac{1}{N}\sum_{i=1}^{N}(y_i - x_i) \tag{5}$$

$$\mathrm{RMSE} = \sqrt{\frac{1}{N}\sum_{i=1}^{N}(y_i - x_i)^2} \tag{6}$$

$$\mathrm{MRE} = \frac{1}{N}\sum_{i=1}^{N}\frac{(y_i - x_i)}{x_i} \times 100 \tag{7}$$

$$\mathrm{RMSRE} = \sqrt{\frac{1}{N}\sum_{i=1}^{N}\left(\frac{y_i - x_i}{x_i}\right)^2} \times 100 \tag{8}$$

where x_i is the reference data (BIV velocity) and y_i is the measured data (FOR velocity) for this velocity comparison. Note that the MBE and RMSE of the measurements give information in the same units as the variable of interest, while the MRE and RMSRE provide more meaningful comparison of errors across the populations (i.e. oil droplets generated from different nozzles).

The velocity (W) comparison by plotting W_{BIV} against W_{FOR} is shown in figure 5, and the statistical errors in the comparison are summarized in table 4. The results indicate that the FOR technique is capable of measuring oil droplet velocity with good accuracy. The RMSE is about 1 cm s^{-1} and the RMSRE is less than 8% for all three cases. The error in the present oil droplet velocity measurements is comparable to the RMSE value of 1.7 cm s^{-1} in the air–water flow reported by Lim *et al* [23]. Interestingly, the RMSE values of the oil droplets seem independent of the velocity magnitude, at least over the range tested. The same observation on bubble velocities was also reported in Lim *et al* [23].

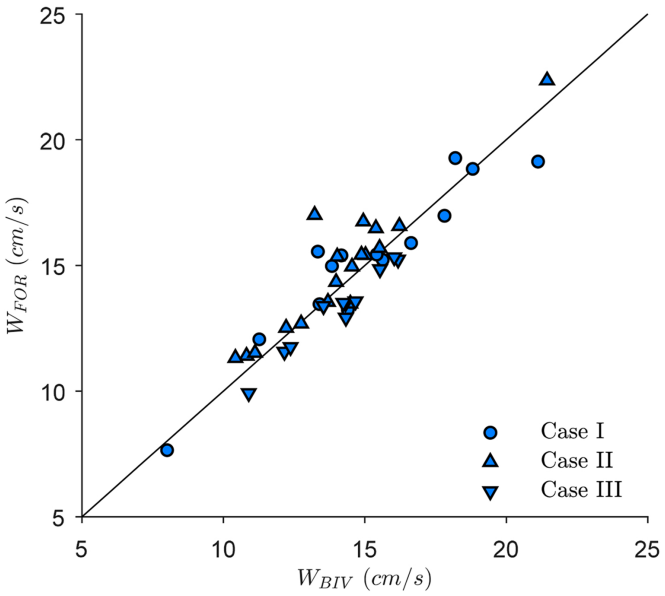

Figure 5. Comparison of the oil droplet rising velocity determined by BIV measurements (W_{BIV}) as a reference velocity and FOR signal processing (W_{FOR}). Note that the *solid line* indicates the 45° expected values.

Table 4. Statistical errors in the velocity comparison.

W data	MBE (cm s^{-1})	RMSE (cm s^{-1})	MRE (%)	RMSRE (%)
Case I	0.1	1.1	0.9	7.6
Case II	0.7	1.2		
Case III	−0.8	0.9		

It should be emphasized that the present approach only requires a single optical-fiber probe for velocity determination. Compared with the dual-probe [35] and quadruple-probe [37, 38], approaches for oil droplet velocity measurements, the single-probe approach not only minimizes the interference in the flow, but also eliminates the need to identify encountered droplets. It largely increases the feasibility of the applications in various fields since the viscosity of oil would affect the velocity measurements more significantly when using multiple-fiber probes. While no direct velocity comparison from results measured by multiple optical fibers and images in oil–water mixture flows is available [24], reported a direct velocity comparison using dual/quadruple-optical-fiber probes and images for air bubbles in a water column. From their results, the MRE between the results using dual- and quadruple-optical-fiber probes against images were up to −8% and 13%, respectively, depending on the air bubble sizes. Moreover, the standard deviations from the velocity measurements by the dual-optical-fiber probe, quadruple-optical-fiber probe, and camera were up to 9.8, 10.6, and 8.4 cm s^{-1}, respectively. They also pointed out that the deformation of the bubble surface by the piercing of the probe causes bubble velocity reduction and the deformation is more obvious for larger bubbles. In contrast, using a single optical fiber, no velocity reduction due to deformation or dependency on the size of oil droplets was noticeably found.

4. Estimation of oil droplet size

As shown in figure 4, coherent mixing of reflected signals from the fiber end-tip face and a moving object in front of the fiber tip provides the velocity information of the object. Lim *et al* [23] demonstrated that the contact angle is nearly normal and the bubble velocity can be determined if the FOR tip penetrates near the center of a bubble. They further showed that, in such a condition, the measured chord length represents the diameter of the bubble if the bubble is spherical (or the minor axis for an ellipsoidal bubble). In their work, the chord-length measurement of air bubbles was calculated by multiplying the measured air bubble velocity with the air-phase residence time, with both values derived from the same FOR signal. The same concept may still be applicable to the chord-length measurements for oil droplets. The oil droplet velocity determination has been described in the previous section, and the determination of the oil-phase residence time will be introduced below. After that, the presentation of chord length measurements will be given. Moreover, the droplet–probe interaction will be discussed to investigate the lower limit of the measurable range using this technique for oil droplet sizing.

4.1. Residence time of oil phase

The residence time of the oil phase can be determined using the moments of entry and exit of an oil droplet in the FOR signal time series. As mentioned earlier, negative, fluctuating, and non-bell-shaped oscillating signals were present in the FOR measurements of the oil–water mixture flow, leading to underestimation of oil phase residence time and/or overestimation of encounter frequencies if the single-threshold detection method that has been applied to air bubble measurements is employed here. To address this issue, the concept of a Schmitt trigger using double thresholds was combined to extract the time window of the oil droplet passage through the fiber tip. The concept of the Schmitt trigger is to obtain square waves from the noisy signal using double thresholds. For example, the processed signal stays at zero until the FOR signal passes the upper threshold and the processed signal stays at one until the FOR signal passes the lower threshold. In this method, the mean (m_{w}) and standard deviation (s_{w}) of the water-phase FOR signal were used to define the upper threshold and lower threshold as $m_{\mathrm{w}} + 4s_{\mathrm{w}}$ and $m_{\mathrm{w}} - 4s_{\mathrm{w}}$, respectively. Then, both thresholds were applied to identify oil droplet encounters.

Even though the double-threshold method worked well in most scenarios, it is possible for multiple processed signals to occur in a single droplet encounter in such signals as shown in figures 3(c)–(d). This would underestimate the residence time and overestimate the encounter frequency. To avoid this, the mean residence time was initially calculated using the double-threshold method. The multiple processed signals in a measured residence time less than one-quarter of the mean residence time were removed. An example of signal processing using the double-threshold method is shown in figure 3 presented in section 2.3. The disadvantage of this method is that the residence time after signal processing will represent

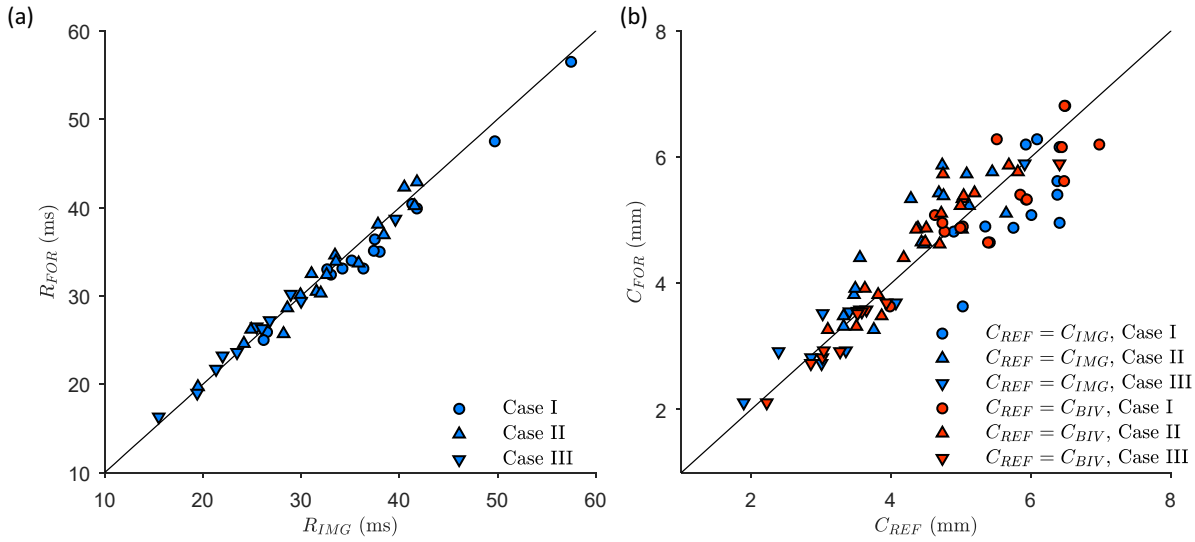

Figure 6. (a) Comparison of the residence time obtained by FOR (R_{FOR}) and images (R_{IMG}). (b) Comparison of the chord length obtained by FOR signals (C_{FOR}) and high-speed images (C_{REF}). Note that *solid lines* indicate the 45° expected values for (a) and (b).

a single oil droplet in cases in which the consecutive encounters of oil droplets are less than one-quarter of the mean measured residence time apart. This could lead to overestimation of the residence time but also implies there may be a limitation on highly concentrated oil–water mixture flows. A better convergence test would improve accuracy in future work, especially for a very high oil concentration flow.

With the processed FOR signal available, such as the *dashed lines* in figure 3, the residence time for each oil droplet encounter can be readily extracted and collected. To verify the robustness of the double-threshold method, the result was further compared with that obtained from corresponding high-speed images. As mentioned earlier, the temporal resolution is 2000 μs for the recorded images. An effort was made to interpolate to match up the measured residence times from images and those from the FOR signal. The image gradient method, an edge-detection technique by detecting the change of image intensity, was applied to obtain interfaces at the moments of entry and exit of oil droplets along the axis of the optical fiber. The comparison is plotted in figure 6(a), with all data points close to the expected straight line. Table 5 summarizes statistical errors for the residence time (R) from the FOR signal (R_{FOR}) as the measured data and images (R_{IMG}) as the reference data. Based on the results, the FOR technique has a capability of measuring the residence time at high accuracy with an RMSRE error of about 4%.

4.2. Chord-length measurements

With the oil droplet rising velocity (W_{FOR}) and oil-phase residence time (R_{FOR}) measured, the chord length can be calculated accordingly (i.e. $C_{\mathrm{FOR}} = R_{\mathrm{FOR}} W_{\mathrm{FOR}}$). To validate the chord lengths obtained from the FOR signal, two different reference chord lengths (C_{REF}) were used for comparisons: chord length from images (C_{IMG}) and chord length calculated from the measured velocity by BIV measurements (V_{BIV}) and residence time obtained by images (R_{IMG}), i.e. $C_{\mathrm{BIV}} = R_{\mathrm{IMG}} W_{\mathrm{BIV}}$. For C_{IMG} measurements, the chord lengths were directly measured from images using the image gradient method at the interfaces of the cross-section along the axis of the optical fiber before the fiber tip comes into contact with oil droplets. C_{IMG} represents the direct chord-length measurements of droplets before the fiber comes into contact with droplets from images, while C_{BIV} represents the indirect chord-length measurements of droplets calculated with the approaching velocity to the fiber by BIV and the residence time from images.

Figure 6(b) plots the chord length derived from the FOR signal (C_{FOR}) against the two reference chord lengths (C_{REF}), C_{IMG} and C_{BIV}. As shown in table 5, the MRE and RMSRE values between C_{FOR} and C_{IMG} were estimated as 0.8%, and 13%, respectively, while those between C_{FOR} and C_{BIV} were estimated as −0.1%, and 7.6%, respectively. The RMSRE values between C_{FOR} and C_{BIV} were slightly smaller than those between C_{FOR} and C_{IMG}. To the authors' knowledge, no direct or indirect chord-length comparisons from optical-fiber signals and images in oil–water mixture flows are available in the literature. Compared to the air–water flow data [23], the RMSE of chord-length measurements in the oil–water mixture flow was about 3 (C_{FOR}–C_{IMG}) and 2 (C_{FOR}–C_{BIV}) times that in the air–water flow (roughly 0.2 mm). In addition, the RMSRE of chord-length measurements in the oil–water mixture flow is similar for the C_{FOR}–C_{IMG} comparison to the RMSE of normalized chord-length results in the air–water flow (11%). Compared to quadruple-optical-fiber data in an aerated flow [24], reported that the MRE of chord lengths from optical-fiber probes and images was −10% which implies that the chord lengths from quadruple optical probes are 10% shorter than those from images. However, the chord-length measurements using a single-optical-fiber probe does not result in significant underestimation of the measured chord lengths (no more than −1% as shown in table 5). This could be an advantage of the FOR technique because the velocity

Table 5. Statistical errors in comparison.

	R, C_{FOR}–C_{IMG}, C_{FOR}–C_{BIV}			
Data	MBE	RMSE	MRE (%)	RMSRE (%)
Case I	−1.4 ms, −0.6 mm, −0.2 mm	1.7 ms, 0.8 mm, 0.5 mm	−1.0, 0.8, −0.1	3.9, 13, 7.6
Case II	−0.1 ms, 0.3 mm, 0.2 mm	1.3 ms, 0.6 mm, 0.4 mm		
Case III	0.3 ms, 0.03 mm, −0.2 mm	0.8 ms, 0.3 mm, 0.2 mm		

Table 6. Categories of droplet–probe interaction.

Category	FOR	HSC	We_m	Ca	D_e/D_{op}
1	Detected	Penetrated	$We_m > 1.7 \times 10^{-2}$	$Ca > 3.7 \times 10^{-3}$	$D_e/D_{op} > 20$
2	Detected	Penetrated; direction changed after penetration	$We_m > 3.2 \times 10^{-3}$ $We_m \leq 1.7 \times 10^{-2}$	$Ca > 2.0 \times 10^{-3}$ $Ca \leq 3.7 \times 10^{-3}$	$D_e/D_{op} > 14$ $D_e/D_{op} \leq 20$
3	Not detected	Not penetrated	$We_m \leq 3.2 \times 10^{-3}$	$Ca \leq 2.0 \times 10^{-3}$	$D_e/D_{op} \leq 14$

measured by the FOR technique is much less affected by the deformation of the bubbles/drops during the penetration process so the error in chord-length measurements can be minimized.

5. Droplet–probe interaction

The velocity, residence time, and chord length measured by the FOR probe were validated with those from images in previous sections for Cases I, II, and III featuring an average droplet diameter greater than 3 mm, as shown in table 1. Nevertheless, the same technique and analysis procedure did not work for droplets generated in Case IV featuring an average diameter less than 2 mm. To evaluate the applicability of the FOR technique in the oil–water mixture flow, droplet–probe interaction is discussed in this section. To find the limit of the technique, the droplet–probe interaction is characterized in terms of the dominating dimensionless parameters based on force balancing during the contact between the optical fiber and the oil droplet. This analysis followed characterization introduced by Vejražka *et al* [44].

The associated dimensionless parameters are the modified Weber number (We_m), representing the ratio between the inertial force of the droplet and the surface tension from the fiber tip, and the capillary number (Ca), representing the ratio between the viscous force and surface tension of the droplet. They can be defined as follows:

$$We_m = \frac{\rho_c U^2 D_e^2}{\sigma D_{op}} \tag{9}$$

$$Ca = WeRe^{-1} = \frac{\mu_c U}{\sigma} \tag{10}$$

where ρ_c is the density of the continuous phase (water in this study), U is the droplet velocity, D_e is the equivalent droplet diameter, σ is the oil–water surface tension, and D_{op} is the diameter of the optical fiber. According to Vejražka *et al* [44], the key parameter of the droplet–probe interaction is We_m, which characterizes the droplet ability to overcome surface-tension forces arising from the contact with the probe tip. On the other hand, Ca characterizes the viscous effect of the oil droplet to be penetrated by the optical-fiber probe. For the calculation of these dimensionless parameters, two essential inputs are required: the equivalent diameter and velocity of the oil droplets. In this study, the equivalent diameter of an oil droplet was measured using the image gradient method and the velocity was measured using the BIV technique.

Table 6 summarizes the categories of applicability for droplet–probe interaction based on the measurements from the FOR signal and observations from the HSC images. Category 1 represents the region in which the optical fiber penetrates the oil droplet and the FOR signal clearly shows the entry and exit of the encountered oil droplet. For Category 2, the optical fiber penetrates the oil droplet, but the direction of the oil droplet is altered after the penetration, implying that the inertia force of the droplet is insufficient to overcome the surface tension during the contact. In this category, FOR signals were unable to acquire the entry and exit signals for the encounter. For category 3, there is no penetration and no detected signal was observed in the measurements. In short, Categories 1, 2, and 3 indicate that the FOR technique is capable of obtaining droplet velocity and size, the FOR technique is capable of obtaining droplet velocity but not size, and the FOR technique is not applicable, respectively.

Figure 7 plots We_m and Ca against the equivalent droplet diameter normalized by the optical fiber diameter, D_e/D_{op}. From table 6 and figure 7, the minimum measurable diameter of the oil droplets is about 20 times the optical fiber diameter which corresponds to about 2.5 mm. Based on the signals and images, the droplet–optical-fiber contacts in Category 2 show that the FOR signal was detected but the optical fiber did not entirely penetrate the oil droplets. Compared with the modified Weber and capillary numbers, all We_m values less than and equal to 1.7×10^{-2} are in the region where D_e/D_{op} is less than or equal to 20, whereas Ca values less than 3.7×10^{-3} are not always in the region where D_e/D_{op} is less than or equal to 20. This could imply that the ability of penetration of the optical fiber is more dominant in the inertial force of the oil droplet to overcome the surface tension on the optical-fiber tip rather

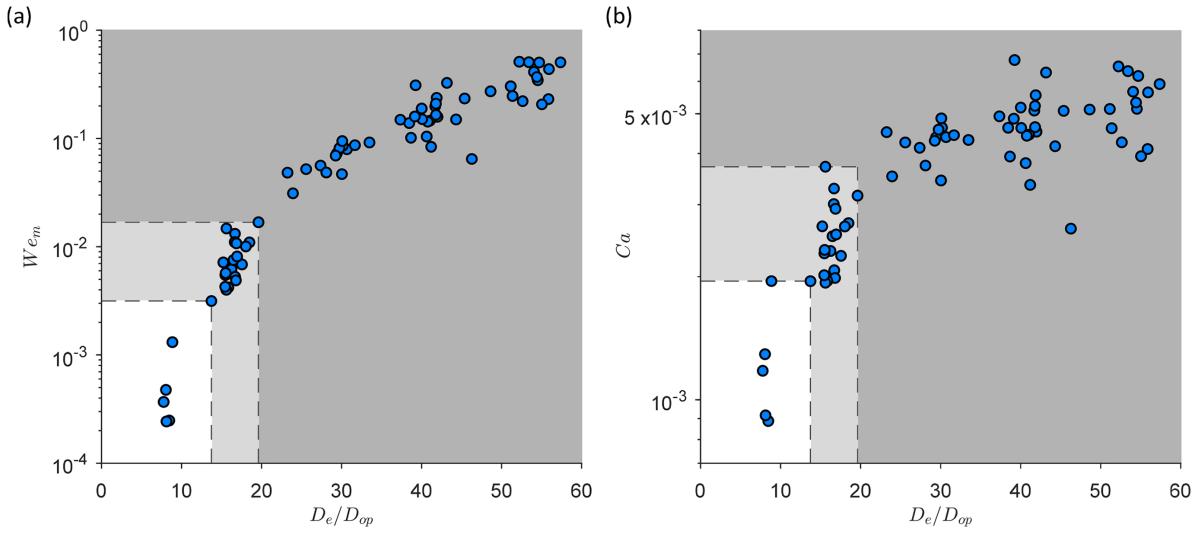

Figure 7. (a) Relationship between normalized equivalent droplet diameter by optical fiber diameter (D_e/D_{op}) and modified Weber number (We_m); (b) relationship between D_e/D_{op} and Capillary number (Ca). Note that Categories 1, 2, and 3 are in the grey, light grey, and white areas, respectively.

than the viscous force of the oil droplet to the oil–water surface tension. Note that the optical fiber used in the present study has a cleaved-tip feature. If the tip were etched into a sharp tip, the minimum measurable diameter might be reduced. Further studies are needed on expanding the applicability region by sharpening the fiber tip.

It should also be pointed out that, even though the rate of analyzable encounters is very low (approximately 1%, as presented in section 3.2) for oil droplets, the FOR technique is indeed one of the few techniques that are capable of measuring the droplet velocity and size *in situ* and simultaneously. The single-probe FOR technique is able to obtain only the droplet chord length which represents the actual droplet diameter. In comparison with image-based methods, the FOR technique is not affected by the droplet concentration; it is free from the overlapping effect created by high droplet concentration. In contrast, the dual and quadruple probes are able to measure droplet velocity and chord length, although the data may suffer from reliability and accuracy due to probe obstruction. However, the measured chord length does not represent, and probably cannot be used to obtain, the actual droplet diameter.

6. Conclusions

The FOR technique is capable of measuring the approaching velocity of an oil droplet using coherently beating signals when the droplet is on the axis of the optical fiber and the fiber penetrates near the center of the droplet. The residence time of the droplet can also be obtained by analyzing the phase changes in the signal. The droplet chord length, which is essentially its diameter, can be subsequently derived. While the residence time measurement is intrusive, the velocity measurement is non-intrusive because the technique measures the approaching velocity before the optical fiber influences the droplet motion and penetrates the droplet. The droplet velocity and chord-length measurements from FOR were validated with measurements directly obtained from images.

The limit of measurable droplet size was investigated using the dominant dimensionless parameters—the modified Weber number and the capillary number. The result indicates that there is a certain lower limit of detection for this technique. For the present cleaved-tip optical fiber employed for the droplet size measurement, the lower limit of measurable droplet diameter was found to be about 20 times the diameter of the optical-fiber probe. This study concludes that the velocity and size of oil droplets in an oil–water mixture flow can be measured using a cleaved-tip single optical fiber for oil droplets with diameter bigger than 2.5 mm. Compared with the use of dual or quadruple probes, the FOR technique with a single probe can minimize the interference and uncertainty during its contact with oil droplets in both velocity and size measurements.

Acknowledgments

The authors wish to thank Professor Scott Socolofsky for providing the oil used in the experiment.

ORCID iD

Kuang-An Chang https://orcid.org/0000-0003-3177-4896

References

[1] Johansen Ø, Rye H and Cooper C 2003 DeepSpill—-field study of a simulated oil and gas blowout in deep water *Spill Sci. Technol. Bull.* **8** 433–43

[2] Tan S K and Yao A 2001 Recognition and measurement of dispersed oil droplets in a water column *J. Hydraul. Res.* **39** 99–103

[3] Lunel T 1993 Dispersion: oil droplet size measurements at sea *Int. Oil Spill Conf.* (American Petroleum Institute) pp 794–5

[4] Brandvik P J, Johansen Ø, Leirvik F, Farooq U and Daling P S 2013 Droplet breakup in subsurface oil releases–Part 1: experimental study of droplet breakup and effectiveness of dispersant injection *Mar. Pollut. Bull.* **73** 319–26

[5] Zhao L, Shaffer F, Robinson B, King T, D'Ambrose C, Pan Z, Gao F, Miller R S, Conmy R N and Boufadel M C 2016 Underwater oil jet: hydrodynamics and droplet size distribution *Chem. Eng.* J. **299** 292–30

[6] Boxall J A, Koh C A, Sloan E D, Sum A K and Wu D T 2010 Measurement and calibration of droplet size distributions in water-in-oil emulsions by particle video microscope and a focused beam reflectance method *Ind. Eng. Chem. Res.* **49** 1412–8

[7] Neal L and Bankoff S 1963 A high resolution resistivity probe for determination of local void properties in gas–liquid flow *AlChE J.* **9** 490–4

[8] Van Der Welle R 1985 Void fraction, bubble velocity and bubble size in two-phase flow *Int. J. Multiphase Flow* **11** 317–45

[9] Lucas G, Mishra R and Panayotopoulos N 2004 Power law approximations to gas volume fraction and velocity profiles in low void fraction vertical gas–liquid flows *Flow Meas. Instrum.* **15** 271–83

[10] Zhai L-S, Bian P, Gao Z-K and Jin N-D 2016 The measurement of local flow parameters for gas–liquid two-phase bubbly flows using a dual-sensor probe array *Chem. Eng. Sci.* **144** 346–63

[11] Cartellier A 1990 Optical probes for local void fraction measurements: characterization of performance *Rev. Sci. Instrum.* **61** 874–86

[12] Cartellier A 1992 Simultaneous void fraction measurement, bubble velocity, and size estimate using a single optical probe in gas–liquid two-phase flows *Rev. Sci. Instrum.* **63** 5442–53

[13] Cartellier A and Achard J L 1991 Local phase detection probes in fluid/fluid two-phase flows *Rev. Sci. Instrum.* **62** 279–303

[14] Saberi S, Shakourzadeh K, Bastoul D and Militzer J 1995 Bubble size and velocity measurement in gas—liquid systems: application of fiber optic technique to pilot plant scale *Can. J. Chem. Eng.* **73** 253–7

[15] Rinne A and Loth R 1996 Development of local two-phase flow parameters for vertical bubbly flow in a pipe with sudden expansion *Exp. Therm. Fluid. Sci.* **13** 152–66

[16] Cartellier A 1998 Measurement of gas phase characteristics using new monofiber optical probes and real-time signal processing *Nucl. Eng. Des.* **184** 393–408

[17] Serdula C D and Loewen M R 1998 Experiments investigating the use of fiber-optic probes for measuring bubble-size distributions *IEEE J. Oceanic Eng.* **23** 385–99

[18] Barrau E, Riviere N, Poupot C and Cartellier A 1999 Single and double optical probes in air–water two-phase flows: real time signal processing and sensor performance *Int. J. Multiphase Flow* **25** 229–56

[19] Kiambi S L, Duquenne A M, Bascoul A and Delmas H 2001 Measurements of local interfacial area: application of bi-optical fibre technique *Chem. Eng. Sci.* **56** 6447–53

[20] Chang K-A, Lim H-J and C B S 2003 Fiber optic reflectometer for velocity and fraction ratio measurements in multiphase flows *Rev. Sci. Instrum.* **74** 3559–65

[21] Chang K-A, Lim H-J and Su C B 2004 Reply to 'Comment on "Fiber optic reflectometer for velocity and fraction ratio measurements in multiphase flows"' [Rev. Sci. Instrum. 74, 3559 (2003)] *Rev. Sci. Instrum.* **75** 286

[22] Juliá E J, Harteveld W K, Mudde R F and Van den Akker H E A 2005 On the accuracy of the void fraction measurements using optical probes in bubbly flows *Rev. Sci. Instrum.* **76** 035103

[23] Lim H J, Chang K A, Su C B and Chen C Y 2008 Bubble velocity, diameter, and void fraction measurements in a multiphase flow using fiber optic reflectometer *Rev. Sci. Instrum.* **79** 125105

[24] Xue J L, Al-Dahhan M, Dudukovic M P and Mudde R F 2008 Four-point optical probe for measurement of bubble dynamics: validation of the technique *Flow Meas. Instrum.* **19** 293–300

[25] Sakamoto A and Saito T 2012 Robust algorithms for quantifying noisy signals of optical fiber probes employed in industrial-scale practical bubbly flows *Int. J. Multiphase Flow* **41** 77–90

[26] Saito T and Toriu M 2015 Effects of a bubble and the surrounding liquid motions on the instantaneous mass transfer across the gas–liquid interface *Chem. Eng.* J. **265** 164–75

[27] Chaumat H, Billet-Duquenne A M, Augier F, Mathieu C and Delmas H 2005 Application of the double optic probe technique to distorted tumbling bubbles in aqueous or organic liquid *Chem. Eng. Sci.* **60** 6134–45

[28] Neto I E L, Zhu D Z and Rajaratnam N 2008 Air injection in water with different nozzles *J. Environ. Eng-ASCE* **134** 283–94

[29] Wang F, Jin N D, Wang D Y, Han Y F and Liu D Y 2017 Measurement of gas phase characteristics in bubbly oil–gas–water flows using bi-optical fiber and high-resolution conductance probes *Exp. Therm. Fluid. Sci.* **88** 361–75

[30] Zhao D, Guo L, Hu X, Zhang X and Wang X 2006 Experimental study on local characteristics of oil–water dispersed flow in a vertical pipe *Int. J. Multiphase Flow* **32** 1254–68

[31] Lucas G P and Panagiotopoulos N 2009 Oil volume fraction and velocity profiles in vertical, bubbly oil-in-water flows *Flow Meas. Instrum.* **20** 127–35

[32] Lucas G P and Zhao X 2013 Large probe arrays for measuring mean and time dependent local oil volume fraction and local oil velocity component distributions in inclined oil-in-water flows *Flow Meas. Instrum.* **32** 76–83

[33] Han Y F, Jin N D, Zhai L S, Zhang H X and Ren Y Y 2017 Flow pattern and holdup phenomena of low velocity oil–water flows in a vertical upward small diameter pipe *J. Pet. Sci. Eng.* **159** 387–408

[34] Hamad F A, Imberton F and Bruun H H 1997 An optical probe for measurements in liquid–liquid two-phase flow *Meas. Sci. Technol.* **8** 1122–32

[35] Hamad F A, Pierscionek B K and Bruun H H 2000 A dual optical probe for volume fraction, drop velocity and drop size measurements in liquid–liquid two-phase flow *Meas. Sci. Technol.* **11** 1307–18

[36] Hamad F A and He S 2010 Evaluation of hot-film, dual optical and Pitot tube probes for liquid–liquid two-phase flow measurements *Flow Meas. Instrum.* **21** 302–11

[37] Yuan Y and Gao Y 2017 A study on hydrodynamic characteristics in a Φ38 pulsed extraction column by four-sensor optical fiber probe *AlChE J.* **63** 801–11

[38] Sun Y D, Gao Y, Hou H G, Jiao C S, Zhou Y and Zhang M 2019 Study on droplet velocity in a pulsed sieve plate extraction column by four-sensor optical fiber probe *Chem. Eng. Res. Des.* **144** 550–8

[39] Chuang W-L, Chang K-A and Mercier R 2017 Impact pressure and void fraction due to plunging breaking wave impact on a 2D TLP structure *Exp. Fluids* **58** 68

[40] Chuang W-L, Chang K-A and Mercier R 2018 Kinematics and dynamics of green water on a fixed platform in a large wave basin in focusing wave and random wave conditions *Exp. Fluids* **59** 100

[41] Fordham E J, Holmes A, Ramos R T, Simonian S, Huang S M and Lenn C P 1999 Multi-phase-fluid discrimination with

local fibre-optical probes: I. Liquid/liquid flows *Meas. Sci. Technol.* **10** 1329–37
[42] Born M and Wolf E 1999 *Principles of Optics* (Cambridge: Cambridge University Press)
[43] Ryu Y, Chang K A and Lim H J 2005 Use of bubble image velocimetry for measurement of plunging wave impinging on structure and associated greenwater *Meas. Sci. Technol.* **16** 1945–53
[44] Vejražka J, Večeř M, Orvalho S, Sechet P, Ruzicka M C and Cartellier A 2010 Measurement accuracy of a mono-fiber optical probe in a bubbly flow *Int. J. Multiphase Flow* **36** 533–48